Journal of Hazardous Materials 199–200 (2012) 1–8

Contents lists available at SciVerse ScienceDirect

Journal of Hazardous Materials

journal homepage: www.elsevier.com/locate/jhazmat

Design of polyoxometallate–titania composite film ($H_3PW_{12}O_{40}/TiO_2$) for the degradation of an aqueous dye Rhodamine B under the simulated sunlight irradiation

Nan Lu [a], Yahui Zhao [a], Hongbo Liu [b], Yihang Guo [a], Xing Yuan [a,*], Hui Xu [a], Huifang Peng [a], Hongwei Qin [a]

[a] School of Urban and Environmental Sciences, Northeast Normal University, Changchun 130024, PR China
[b] Changchun Institute of Optics, Fine Mechanics and Physics, Chinese Academy of Sciences, Changchun 130033, PR China

ARTICLE INFO

Article history:
Received 11 April 2011
Received in revised form 22 July 2011
Accepted 29 August 2011
Available online 3 September 2011

Keywords:
Polyoxometallate
Titania
Composite film
Photocatalysis
Simulated sunlight

ABSTRACT

A series of polyoxometallate/titania ($H_3PW_{12}O_{40}/TiO_2$) composite films with different $H_3PW_{12}O_{40}$ loadings (6.3%, 7.7%, 14.7% and 16.7%) were prepared by a modified sol–gel-hydrothermal route followed by a spin-coating method. The smooth films are constructed by the well-distributed $H_3PW_{12}O_{40}/TiO_2$ sphere with particle size in the range from 80 to 100 nm, and the bandgap of the composite films is somewhat narrower compared with as-prepared pure TiO_2 film. As a novel photocatalytic material, the photocatalytic performances of the $H_3PW_{12}O_{40}/TiO_2$ composite films were evaluated by the degradation and mineralization of an aqueous dye Rhodamine B (RB) under solar simulating Xe lamp irradiation ($320\,nm < \lambda < 780\,nm$), and the enhanced photocatalytic activity in comparison to pure TiO_2 film as well as the $H_3PW_{12}O_{40}/TiO_2$ and Degussa P25 TiO_2 powder was obtained. Additionally, the composite films can be reused at least for three times without losing their catalytic activity.

1. Introduction

Since the development of photocatalysis technology, titanium dioxide photocatalyst has been investigated extensively due to its low cost, non-toxicity, high stability and great efficiency in degrading difficult-to-remove organic pollutants of wastewater [1–5]. However, the photocatalytic efficiency of TiO_2 is limited due to: (i) the high recombination ratio of photogenerated electrons (e^-) and holes (h^+) on the surface of TiO_2 under ultraviolet (UV) light irradiation; and (ii) null photoresponse of TiO_2 under visible light irradiation, which severely limits on the development of solar photocatalysis for environmental applications [6]. Accordingly, lots of efforts have been made to enhance the photocatalytic activity of TiO_2 via the modification with different materials such as transition metals [7,8], nonmetal atoms [9–11], other semiconductors [12,13], and noble metals [14–16]. In recent years, some polyoxometallates (POMs) supported on TiO_2 composite materials as heterogeneous photocatalysts have been reported successively and exhibit relatively higher photocatalytic degradation abilities towards aqueous organic pollutants [17–23]. As a kind of widely used POMs in homogeneous acid- and photo-catalytic reactions, $H_3PW_{12}O_{40}$ (12-tungstophosphoric acid) is a very strong Brösted acid and efficient electron trap with well-defined Keggin structure [24–26]. $H_3PW_{12}O_{40}$ shares very similar photochemical characteristics with semiconductor photocatalysts. Therefore, $H_3PW_{12}O_{40}$ should be an excellent candidate for delaying the fast e^-–h^+ recombination on the surface of TiO_2 and improving the photocatalytic activity due to its intrinsic electronic attribute.

Nevertheless, current studies on photocatalysis are mainly based on powder-type photocatalysts, which severely hindered their practical applications due to the post-treatment problems in these systems such as separation, recovery and reuse. To overcome these disadvantages, much attention has been paid to explore immobilized TiO_2-based film materials [27–29]. Among all kinds of the methods to prepare TiO_2-based thin film, the sol–gel method has been used extensively [30,31]. However, further thermal treatment at a high temperature (500–600 °C) is generally needed for the film materials obtained by the sol–gel method in order to induce crystallization. The process significantly affects morphology of the film materials including the increased particle size, the decreased specific surface area, and sometimes the surface crack of the film, which reduce the contact of reactant and the active site and thereby hindering the preparation and utilization of TiO_2-based thin film photocatalysts [30,32,33]. Accordingly, the development

* Corresponding author. Tel.: +86 431 85099561; fax: +86 431 85099561.
E-mail address: yuanx@nenu.edu.cn (X. Yuan).

0304-3894/$ – see front matter © 2011 Elsevier B.V. All rights reserved.
doi:10.1016/j.jhazmat.2011.08.070

of a method without the calcination step for crystallization of amorphous TiO_2 may be more favorable to improve the photocatalytic performances of the TiO_2-based film materials. On the other hand, previous work concerning the photocatalytic activity of the POM/TiO_2 composite films was evaluated under UV-light irradiation by using high pressure mercury lamp as a light source [34,35], which results in the technique lack of practical significance.

Herein, a series of $H_3PW_{12}O_{40}/TiO_2$ composite film photocatalysts were designed and prepared via the modified sol–gel-hydrothermal route followed by a spin-coating method for the first time. The method can ensure the film with perfect anatase phase structure obtained at low temperature (473 K). The composition and structure, morphology, and optical absorption property of as-prepared materials were well-characterized. Subsequently, the photocatalytic performances of the $H_3PW_{12}O_{40}/TiO_2$ composite films were evaluated by the degradation and mineralization of an aqueous dye Rhodamine B (RB) under solar simulating Xe lamp irradiation (320 nm < λ < 780 nm). By using this kind of light source, the degradation process is more similar to that of the practical process proceeds under the natural sunlight. RB, widely exists in dye wastes, is a kind of typical organic pollutant, and it can severely affect environment and human health due to its high toxicity [36]. Moreover, RB is hard to be degraded completely by conventional methods. Therefore, the studies for such pollutant on searching for alternative and efficient treatment processes are urgent. During the photocatalytic degradation of RB, the influences of various parameters such as the loadings of $H_3PW_{12}O_{40}$, initial concentration of dye solution, pH value of the solution on the photocatalytic performances of $H_3PW_{12}O_{40}/TiO_2$ composite films were investigated; meanwhile, the composite films were compared with as-prepared $H_3PW_{12}O_{40}/TiO_2$ composite powder as well as Degussa P25 TiO_2 powder. Finally, the recyclability of the composite films was tested by three times' RB degradation run.

2. Experimental

2.1. Catalyst preparation

A typical preparation method of $H_3PW_{12}O_{40}/TiO_2$ composite film is described below. A titanium tetraisopropoxide (TTIP) solution (denoted as A) was prepared by dropping TTIP (2 mL) into isopropanol (6 mL) under vigorous stirring for 1 h. The desired amount of $H_3PW_{12}O_{40}$ (0.02, 0.03, 0.05 and 0.06 mmol) was dissolved with isopropanol (1.6 mL), and the resulting $H_3PW_{12}O_{40}$ solution was ultrasonic for 10 min to obtain good dispersion of $H_3PW_{12}O_{40}$ in an isopropanol solvent (denoted as B). After that, B was added dropwise into A under vigorous stirring. And then an adequate acetic acid solution was added for slowing down the hydrolysis rate of TTIP. The resulting mixture was adjusted to pH 2–3 by HCl (2 mol L^{-1}). After stirring for 1 h at room temperature, a white transparent sol was obtained, and then it was transferred into a 25 mL Teflon-lined autoclave and heated to 473 K with a heating rate of 2 K min^{-1}. After keeping constant temperature for 2 h, the temperature was decreased to room temperature at a cooling rate of 1 K min^{-1}. The resulting hydrogel was transferred into a 50 mL beaker and stirred for spin-coating on quartz substrate. Prior to using, each quartz substrate (50 mm × 15 mm × 1 mm) was cleaned in an ultrasound bath for 30 min in turn with detergent, ethanol, and distilled water, and finally dried at 333 K. The composite films were deposited by spin-coating. For each film, the time of dripping solution on quartz was 9 s at 500 rpm, whereas the spin coating had been performed for 10 s at 2000 rpm. Then the film was aged at 293 K for 7 d. The obtained composite film is denoted as $H_3PW_{12}O_{40}/TiO_2$-*x* with *x* representing $H_3PW_{12}O_{40}$ loadings. For comparison, pure TiO_2 film was prepared by using current method in the absence of $H_3PW_{12}O_{40}$.

2.2. Catalyst characterization

Loading of $H_3PW_{12}O_{40}$ in the products was determined by a Leeman Prodigy Spec inductively coupled plasma atomic emission spectrometer (ICP-AES). X-ray diffraction (XRD) patterns were obtained on a Rigaku D/max-3c X-ray diffractometer (Cu Kα radiation, λ = 0.154 nm). UV–vis diffuse reflectance spectra (UV–vis/DRS) were recorded on a Cary 500 UV–vis-NIR spectrophotometer. Raman scattering spectra were recorded on a Jobin-Yvon HR 800 instrument with an Ar^+ laser source of 488 nm wavelength in amacroscopic configuration. FT-IR spectra were recorded on a Nicolet Magna 560 IR spectrophotometer. Field-emission scanning electron micrographs (FESEM) were obtained using a JEOL 6340F scanning electron microscope. Transmission electron microscope (TEM), high resolution transmission electron microscope (HRTEM), and selected area electron diffraction (SAED) micrographs were recorded on a JEM-2100F high resolution transmission electron microscope at an accelerating voltage of 200 kV.

2.3. Photocatalytic test

The light source (being placed *ca.* 15 cm above the reactor) was provided by a PLS-SXE300 Xe lamp (300 W, Beijing Trusttech Co. Ltd., China) equipped with an IR cut filter to remove most of IR irradiation (780–1100 nm). Consequently, the artificial solar light with main emission from 320 nm to 780 nm matches well with the natural solar light (see Fig. S1 of Electronic Supporting Information). The light intensity was adjusted to 200 mW cm^{-2} measured by a radiometer (OPHIR, Newport, USA). In a typical experiment, the ultrasonic aqueous RB solution (25 mg L^{-1}, 120 mL) were poured into a self-designed quartz reactor, and the immobilized composite films (2 pieces of quartz equivalent 4.5 mg powder) was immersed in the RB solution which was kept in the dark under stirring for 30 min in order to achieve adsorption–desorption equilibrium, and then it was irradiated by the Xe lamp. The temperature of the solution was maintained at 303 ± 2 K by circulation water through an external cooling jacket (see Fig. S2 of Electronic Supporting Information). At given intervals of irradiation, fixed amounts of reaction solution were taken out and analyzed by a Shimadzu double-beam spectrophotometer UV-190 at λ = 554 nm, while total organic carbon (TOC) was monitored by a Shimadzu TOC-500 Total Organic Carbon analysis system.

3. Results and discussion

3.1. Preparation and characterization of the $H_3PW_{12}O_{40}/TiO_2$ composite films

The preparation process of materials is closely related to their morphology, phase structure and special physicochemical properties, therefore it is vital to how to control the influences of various factors. Herein, a modified sol–gel-hydrothermal route followed by a spin-coating method was applied to prepared $H_3PW_{12}O_{40}/TiO_2$ composite film catalysts. During the co-hydrolysis of TTIP and $H_3PW_{12}O_{40}$, the hydrolysis rate was controlled through adding the hydrolysis inhibitor (adequate acetic acid solution), which avoided the aggregation of particles and improved the dispersibility of the catalyst. Additionally, the thermal treatment method with temperature programming was applied to induce crystallization of composite materials, which avoided the formation of particle agglomeration and amorphous phase as well as the decomposition of $H_3PW_{12}O_{40}$ (T > 623 K), and facilitated crystallization growth.

XRD analysis was applied to study the phase structure of as-prepared $H_3PW_{12}O_{40}/TiO_2$ composite films with $H_3PW_{12}O_{40}$ loadings of 6.3%, 7.7%, 14.7% and 16.7%, respectively. For comparison, as-prepared pure TiO_2 film was also tested. Pure TiO_2 film

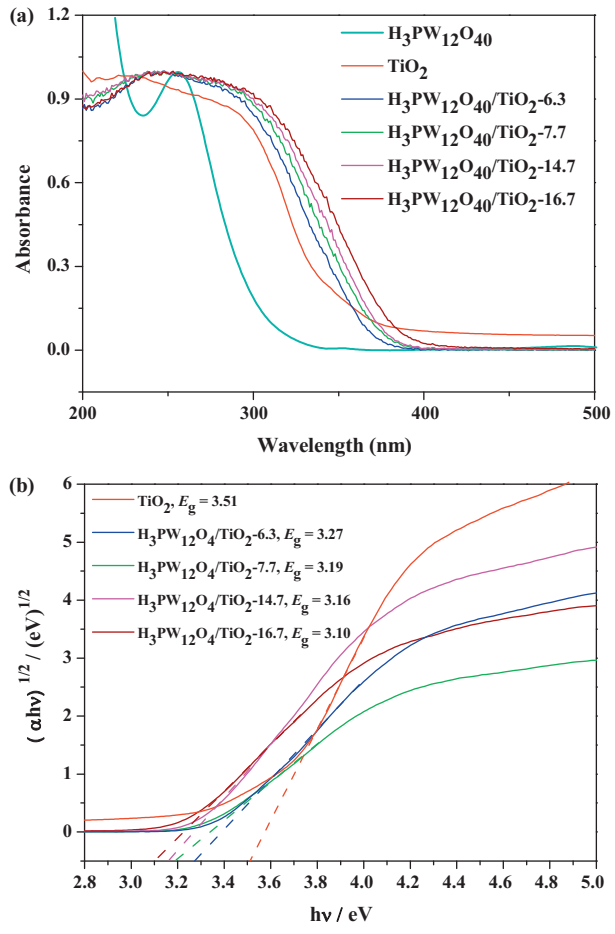

Fig. 1. UV–vis/DRS of the starting $H_3PW_{12}O_{40}$, as-prepared pure TiO_2 film, and $H_3PW_{12}O_{40}/TiO_2$ composite films with different $H_3PW_{12}O_{40}$ loadings.

exhibits anatase phase with the diffraction peaks at 25.3°, 37.8°, 48.0°, 54.4°, and 62.7°, respectively (JCPDS 21-1272). As for the $H_3PW_{12}O_{40}/TiO_2$ composite films, the same characteristic peaks as those of pure TiO_2 film are observed, indicating that the composite films also possess anatase phase (Fig. S3 in Electronic Supporting Information). From the XRD patterns it is also found that the diffractions originated from the Keggin unit are hardly observed for as-prepared composites, implying that the Keggin unit has introduced into TiO_2 network.

In order to investigate the optical properties of the samples, UV–vis/DRS measurements were carried out. The UV–vis/DRS of the starting $H_3PW_{12}O_{40}$, as-prepared pure TiO_2 and $H_3PW_{12}O_{40}/TiO_2$ films are displayed in Fig. 1a. Each TiO_2-based material exhibits a parallel absorption band starting from 260 nm and ending up to *ca.* 400 nm; and the absorption bands of the $H_3PW_{12}O_{40}/TiO_2$ films have an obvious redshift compared with pure TiO_2. More interestingly, the absorption edges of the $H_3PW_{12}O_{40}/TiO_2$ films continuously extend to the longer wavelength as increase $H_3PW_{12}O_{40}$ loadings from 0 to 16.7%. The results indicate that the bandgap of the composite films becomes narrow after the introduction of the Keggin unit into the TiO_2 network. In order to confirm this inference, the bandgap energy (E_g) of the $H_3PW_{12}O_{40}/TiO_2$ composite films and pure TiO_2 thin film were evaluated through Kubelka–Munk formula $\alpha h\nu = A(h\nu - E_g)^{n/2}$, where α, ν, E_g and A are the absorption coefficient, the light frequency, the bandgap and a constant, respectively [36]. From the onsets of the absorption edges as presented in Fig. 1b it can be seen that the bandgap of $H_3PW_{12}O_{40}/TiO_2$ composite material is narrower than that of pure TiO_2 film, which slightly decreases from 3.51 eV to 3.10 eV with the increase of $H_3PW_{12}O_{40}$ loadings from 0 to 16.7%. For pure TiO_2 film, the absorption should be originated from the charge transfer from O 2p to Ti 3d orbit; in the case of the $H_3PW_{12}O_{40}/TiO_2$ composite films, the absorption band is assigned to the charge transfer from O 2p to the new conduction band that is constructed from the hybridization of Ti 3d and W 5d orbit (see Scheme 1) [17]. This is the most important factor to narrow the bandgap of the composite films. Additionally, the increases of the particle sizes with the increasing $H_3PW_{12}O_{40}$ loadings may also lead to the change of the bandgap of the composite films. The result is confirmed by the calculated results through XRD (see Table S2 in Supplementary information). It is also found that no separated absorption peaks corresponding to either $H_3PW_{12}O_{40}$ or TiO_2 are detected in the $H_3PW_{12}O_{40}/TiO_2$ composite films (Fig. 1). The results further confirm that the Keggin unit homogeneously disperses at the atomic level throughout the coupled titania materials without changing the crystal structure of titania.

FT-IR spectroscopy is a very sensitive technique to detect the vibrations of metal–oxygen bonds, and therefore it can provide important information for the structural integrity of the Keggin unit in the $H_3PW_{12}O_{40}/TiO_2$ composites. FT-IR spectra show that the four characteristic vibrational frequencies (700–1100 cm^{-1}) related to the Keggin unit exist in the starting $H_3PW_{12}O_{40}$ and

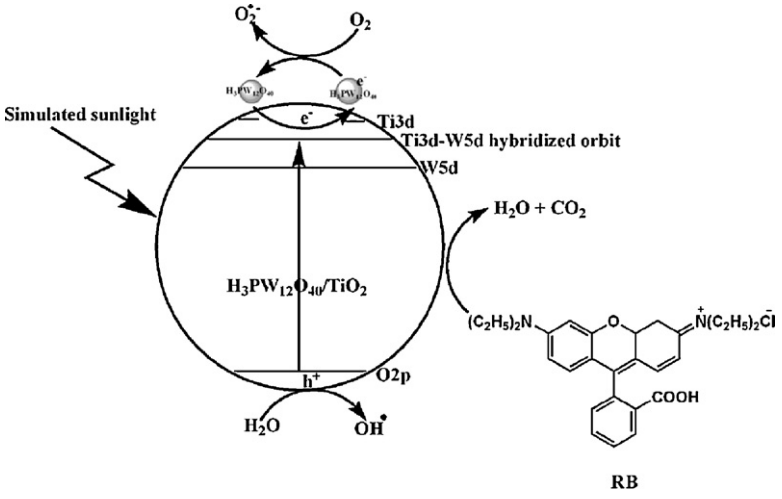

Scheme 1. Photocatalytic cycle of the $H_3PW_{12}O_{40}/TiO_2$ composite film catalyst.

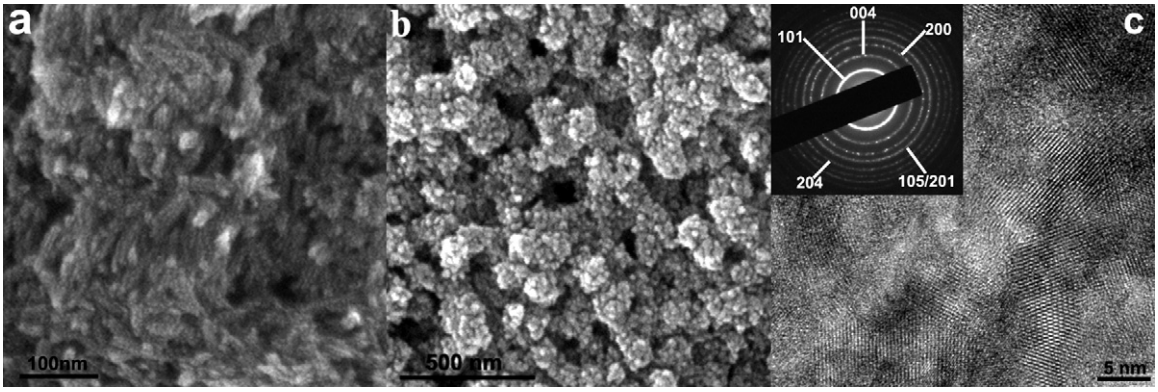

Fig. 2. Field FESEM images of pure TiO_2 film (a) and $H_3PW_{12}O_{40}/TiO_2$-14.7 composite film (b); high-resolution TEM image of $H_3PW_{12}O_{40}/TiO_2$-14.7 (c) and selected area electron diffraction pattern (insert).

$H_3PW_{12}O_{40}/TiO_2$ composite films (Fig. S4 in Electronic Supporting Information), which are assigned to the vibrations of the P–O bonds of the PO_4 units, W=O bonds, and two W–O–W bonds of the Keggin unit [37,38]. Compared with the starting $H_3PW_{12}O_{40}$, the vibrational frequencies of the $H_3PW_{12}O_{40}/TiO_2$ composite films have somewhat shifts, implying that the strong interaction exists in the $H_3PW_{12}O_{40}/TiO_2$ composites although the primary Keggin structure remains intact.

Raman scattering spectroscopy further proves the above conclusion. From the results displayed in the Fig. S5 of Electronic Supporting Information, it can be seen that the starting $H_3PW_{12}O_{40}$ exhibits three Raman scattering peaks situated at 1009 cm^{-1}, 994 cm^{-1}, and 905 cm^{-1}, corresponding to stretching vibrations of P–O bonds of the PO_4 units, W=O bonds, and W–O–W bonds of the Keggin unit, respectively. In the case of as-prepared TiO_2 film, four characteristic Raman scattering peaks found at 149 cm^{-1} (E_g), 402 cm^{-1} (B_{1g}), 518 cm^{-1} (B_{1g}), and 645 cm^{-1} (E_g) originate from anatase TiO_2 [26]. After forming the $H_3PW_{12}O_{40}/TiO_2$ composite films, the Raman scattering peaks related to the Keggin unit are broadened and weakened, and the peak intensity gradually increases with the increasing of $H_3PW_{12}O_{40}$ loadings. Additionally, four anatase TiO_2-related peaks still can be found, however, E_g Raman mode at 149 cm^{-1} shifts to higher wavenumbers, which further implies that strong interaction exists between the Keggin unit and TiO_2 support [22,37,38].

The textural properties of the $H_3PW_{12}O_{40}/TiO_2$ films were evaluated by the nitrogen sorption determination (Fig. S6 of Electronic Supporting Information). From Fig. S6a it can be seen that the isotherms belong to type IV with an H3 hysteresis loop. The result indicates that pure TiO_2 film and $H_3PW_{12}O_{40}/TiO_2$ composite films mainly possess mesoporosity, and that the mesopores are formed due to the aggregation of the product particles. The conclusion is further evidenced by the BJH pore size distribution curves shown in Fig. S6b. That is, wide pore size distribution (9.1–32.7 nm) implies that the pore size of the composite films is less uniform. The calculated textural parameters based on the sorption isotherms are summarized in Table S2. From Table S2 it can be seen the surface areas of the $H_3PW_{12}O_{40}/TiO_2$ composite films increase and then decrease from 169.9 to 137.8 $cm^2\,g^{-1}$ with the increase of $H_3PW_{12}O_{40}$ loadings compared with pure TiO_2 (158.6 $cm^2\,g^{-1}$). As for the pore volume for all tested TiO_2-based films, they are almost in the same value (*ca.* 0.4 $cm^3\,g^{-1}$). The results indicate that during the composite preparation process the Keggin units interact with TiO_2 through Ti–O–W covalent bond to form the $H_3PW_{12}O_{40}/TiO_2$ framework, therefore, the BET surface area increases. However, with the increase of $H_3PW_{12}O_{40}$ loadings, the surface of TiO_2 is saturated, and the residual Keggin units enter into the framework of TiO_2, which makes the BET surface area decrease.

The morphology of as-prepared pure TiO_2 film and $H_3PW_{12}O_{40}/TiO_2$ composite film is revealed by FESEM (Fig. 2a and b) and high-resolution TEM (Fig. 2c) observation. FESEM observation reveals that the films prepared by the sol–gel-hydrothermal route followed by a spin-coating method are stable enough. For pure TiO_2 film, the particles show regular rice shaped with the size of *ca.* 80 nm (Fig. 2a), while the $H_3PW_{12}O_{40}/TiO_2$ particles exhibit well-distributed sphere shaped with particle size of 80–100 nm (Fig. 2b). The above results indicate that the addition of $H_3PW_{12}O_{40}$ into TiO_2 matrix changes the morphology of the TiO_2.

The SAD pattern inserted in Fig. 2c clearly indicates that there is almost no amorphous phase formed. The rings recorded from SAD of the sample, which are indexed to the diffraction from the (1 0 1), (0 0 4), (2 0 0), (1 0 5), and (2 1 1) planes of anatase, are consistent with the above XRD results. The well-crystallized anatase titania with lattice fringe of 0.354 nm can also be seen in this HRTEM image.

3.2. Simulated sunlight photocatalytic performances of the $H_3PW_{12}O_{40}/TiO_2$ film

The simulated sunlight ($320\,nm < \lambda < 780\,nm$) photocatalytic performances of as-prepared $H_3PW_{12}O_{40}/TiO_2$ composite films were evaluated by the degradation of dye RB in an aqueous solution. As a comparison, pure TiO_2 film, $H_3PW_{12}O_{40}/TiO_2$ composite powder as well as Degussa P25 TiO_2 powder were also tested under the same conditions. Meanwhile, the influences of the experimental parameters such as $H_3PW_{12}O_{40}$ loadings, initial RB concentration, and pH value of the system on the photocatalytic performance were also considered.

3.3. Influence of the $H_3PW_{12}O_{40}$ loadings

Fig. 3 shows the effect of the $H_3PW_{12}O_{40}$ loadings on the photocatalytic activity of the $H_3PW_{12}O_{40}/TiO_2$ film towards the degradation of an aqueous RB. It shows that the photocatalytic activity of the $H_3PW_{12}O_{40}/TiO_2$ composite film increases with $H_3PW_{12}O_{40}$ loadings from 0 to 16.7%. Among all tested photocatalytic materials, $H_3PW_{12}O_{40}/TiO_2$-16.7 is the most photoactive, and RB is almost degraded totally after 120 min simulated sunlight irradiation. This result can be explained by the fact that with the increasing $H_3PW_{12}O_{40}$ loadings, the bandgap of the $H_3PW_{12}O_{40}/TiO_2$ composite film becomes narrowed, which gives higher population of the photoexcited electrons and holes to participate in the photocatalytic reaction. Accordingly, more active species that are responsible for the decomposition of RB can be produced. However, $H_3PW_{12}O_{40}/TiO_2$-16.7 film suffers from slight dropping from the quartz substrate during the photocatalytic degradation of RB, while $H_3PW_{12}O_{40}/TiO_2$-14.7 exhibits

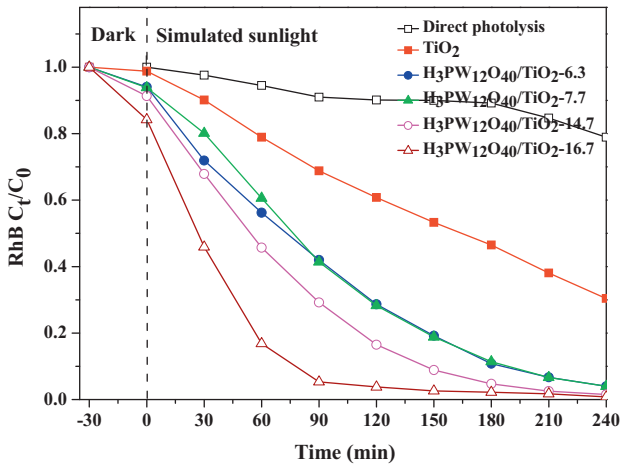

Fig. 3. Photodegradation of dye RB under pure TiO_2 and $H_3PW_{12}O_{40}/TiO_2$ composite films under simulated sunlight irradiation (320 nm < λ < 780 nm). Initial concentration of RB: 25 mg L^{-1}, volume: 120 mL, catalyst amount: two pieces of quartz (4.5 mg).

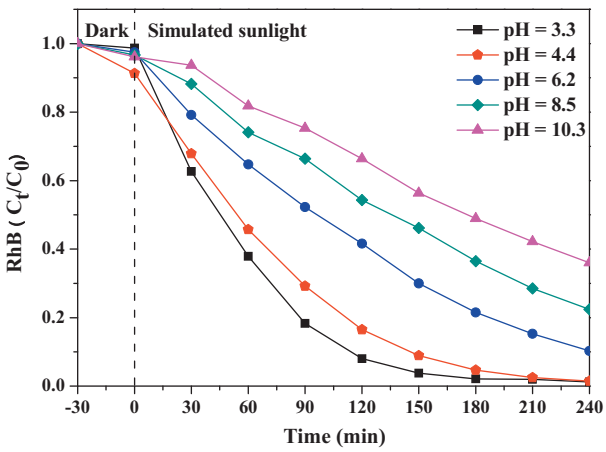

Fig. 5. Influence of the initial pH value on the simulated sunlight photocatalytic activity of the $H_3PW_{12}O_{40}/TiO_2$-14.7 composite film towards RB degradation. Initial concentration of RB: 25 mg L^{-1}, volume: 120 mL, catalyst amount: two pieces of quartz (4.5 mg).

better stability with respect to $H_3PW_{12}O_{40}/TiO_2$-16.7. Therefore, $H_3PW_{12}O_{40}/TiO_2$-14.7 was selected as the representative photocatalyst in subsequent photocatalytic tests. Additionally, for all tested $H_3PW_{12}O_{40}/TiO_2$ composite films, their photocatalytic activities are higher than that of pure TiO_2 film. It is worth noting that only two pieces of quartz slides with the amount of $H_3PW_{12}O_{40}/TiO_2$ of 4.5 mg are used as a photocatalyst in the current system. Thus it can be seen that a small amount of catalyst has been able to receive so good degradation efficiency, which greatly reduces the cost of the experiments. In addition, no separation step is needed for the film catalysts. Thereby, as-prepared POM-containing TiO_2 composite film is expected to be a promising photocatalytic material for the practical applications.

3.4. Effect of the initial RB concentration

The effect of the initial RB concentration on the degradation efficiency was investigated by simulating sunlight irradiating the $H_3PW_{12}O_{40}/TiO_2$-14.7 film (Fig. 4). With the increase of the initial RB concentration from 12.5 mg L^{-1} to 50 mg L^{-1}, the conversion of RB firstly increased and then decreased, and achieved the highest value at initial RB concentration of 37.5 mg L^{-1}. At the fixed $H_3PW_{12}O_{40}$ loading, the photocatalytic performance of

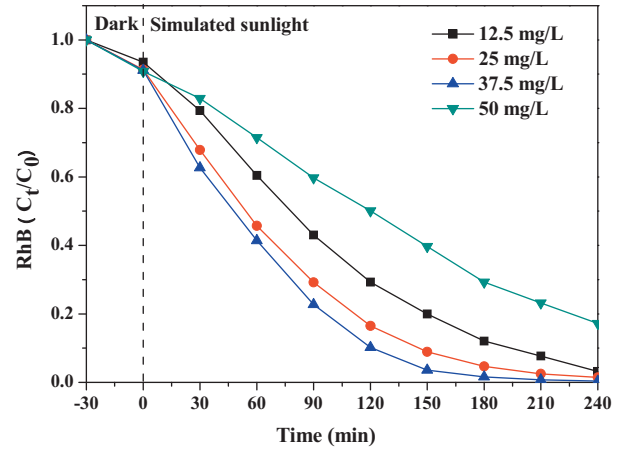

Fig. 4. Influence of the initial RB concentration on the simulated sunlight photocatalytic activity of the $H_3PW_{12}O_{40}/TiO_2$-14.7 composite film. Volume: 120 mL, catalyst amount: two pieces of quartz (4.5 mg).

the $H_3PW_{12}O_{40}/TiO_2$ film is determined by the ratio of the catalytic active sites to the substrate molecules. At relatively lower RB concentrations, catalyst particles are in excess and they can accommodate all RB molecules, therefore, the photocatalytic activity increases with increasing RB concentration and achieves optimal value at a fixed RB concentration. However, when the RB concentration is higher than the optimal value, a competitive adsorption onto the catalyst surface between RB molecules and by-products occurs, thereby fewer active sites are available at higher RB concentrations, leading to poor photocatalytic activities [39].

3.5. Effect of initial pH

Fig. 5 shows the dependence of the photodegradation of RB over the $H_3PW_{12}O_{40}/TiO_2$-14.7 composite film upon different initial pH values (pH = 3.3, 4.4, 6.2, 8.5, 10.3) of the reaction system. It is found that the lower pH values of the reaction system the higher photocatalytic activity of the $H_3PW_{12}O_{40}/TiO_2$-14.7. At pH 3.3, $H_3PW_{12}O_{40}/TiO_2$-14.7 exhibits the highest photodegradation efficiency towards RB; additionally, when pH value is in the range of 3.3–4.4, the degradation rate of RB changes a little. However, in the range of pH 6.2–10.3, the degradation rate of RB is obviously reduced. The above result suggests that the acidic condition is favorable to the degradation of RB molecules in the presence of $H_3PW_{12}O_{40}/TiO_2$-14.7 catalyst. The obviously increased degradation of RB with the decreasing of pH value could be interpreted as follows. On the one hand, in acidic condition, more H^+ adsorb onto the photocatalyst and regenerate the catalyst surface sites through timely removal of the intermediate species from the surface [40], thereby improve the degradation of RB. Additionally, it is well known that the adsorption of the dye onto the catalyst surface directly affects the occurrence of electron transfer between the excited dye and catalyst and further influences the degradation rate. The adsorption experimental results have confirmed that the adsorption capacity of the composite film towards RB molecule significantly decrease with the increase of pH value (Fig. S7). This trend is corresponding to the photodegradation rate of RB at different pH value.

3.6. Comparison of photocatalytic activity of Degussa P25 TiO_2, $H_3PW_{12}O_{40}/TiO_2$ powder, and $H_3PW_{12}O_{40}/TiO_2$ composite film

The photocatalytic activity of three different catalysts including Degussa P25 TiO_2, as-prepared $H_3PW_{12}O_{40}/TiO_2$-14.7 powder

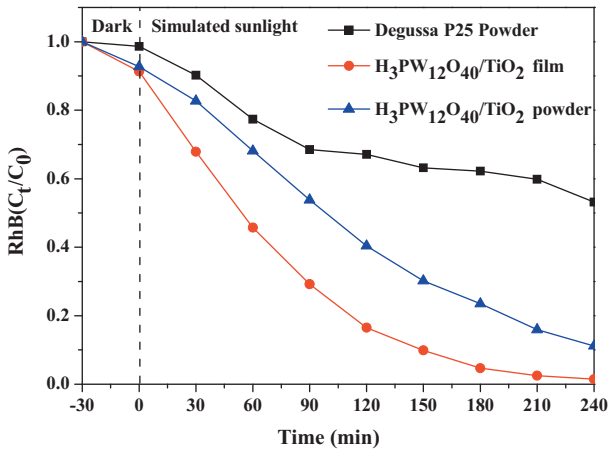

Fig. 6. Photodegradation of RB over simulating sunlight irradiating Degussa P25 TiO_2, $H_3PW_{12}O_{40}/TiO_2$ powder, and $H_3PW_{12}O_{40}/TiO_2$ composite film, respectively. Initial concentration of RB: 25 mg L^{-1}, volume: 120 mL, catalyst amount (0.056 mmol by TiO_2).

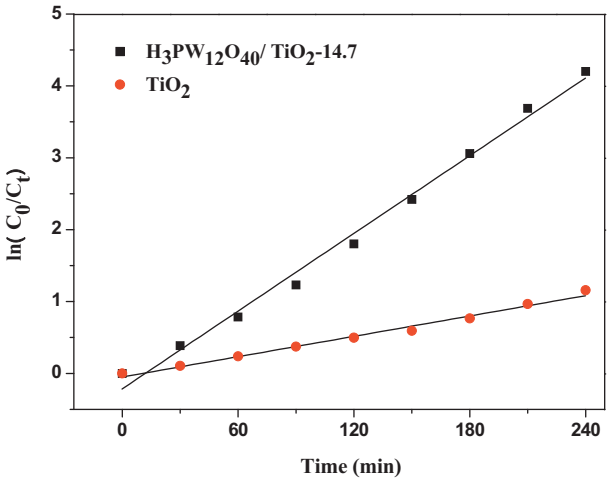

Fig. 7. RB degradation ratio *vs.* irradiation time using composite film and pure TiO_2 film as photocatalyst.

and the composite film with the same mole (0.056 mmol by TiO_2) was compared through the degradation of RB under simulating sunlight irradiation. From the result shown in Fig. 6 it is found that the $H_3PW_{12}O_{40}/TiO_2$ powder is less photoactive than the corresponding film, but the $H_3PW_{12}O_{40}/TiO_2$ powder is more photoactive than Degussa P25 TiO_2. For example, after 240 min simulated sunlight irradiation, RB is almost completely degraded by the $H_3PW_{12}O_{40}/TiO_2$ composite film, however, RB remains 11.2% and 46.9%, respectively, in the $H_3PW_{12}O_{40}/TiO_2$ powder- and Degussa P25 TiO_2 powder-catalyzed reaction system. The unique photocatalytic performance of the composite film with respect to its corresponding powder maybe derive from that too less powder amount (0.056 mmol) relatived to RB aqueous solution (120 mL) decrease the effective contact opportunities between dye molecules and the active sites. Therefore, this adequately highlights the advantages of thin film catalyst compared with powder catalyst.

3.7. Kinetic study

Kinetic study was conducted by selecting pure TiO_2 film and $H_3PW_{12}O_{40}/TiO_2$-14.7 film as the catalysts, and the obtained plots of $\ln(c_0/c_t)$ *vs.* Xe lamp irradiation time are illustrated in Fig. 7. It shows that both plots are nearly straight within 4 h light irradiation, and the linear correlation coefficient I is 0.996 and 0.994 for the $H_3PW_{12}O_{40}/TiO_2$ and TiO_2 film, respectively. The result indicates that the RB degradation reactions follow the apparent first-order kinetic reactions. The reaction rate constant calculated from the plot is 1.8×10^{-2} min^{-1} and 4.7×10^{-3} min^{-1} for the $H_3PW_{12}O_{40}/TiO_2$ and TiO_2 film, respectively, which further confirms that the introduction of the Keggin unit into the TiO_2 framework can accelerate RB degradation rate in comparison to pure TiO_2. The excellent photocatalytic activity of the $H_3PW_{12}O_{40}/TiO_2$ composite film is mainly attributed to the following two reasons. One reason should be attributed to previous reported synergistic effect existed between TiO_2 and the Keggin unit [17,21–23], which results in the retardation of the recombination of the photoexcited h^+–e^- pairs owing to trapping photoexcited electrons into unoccupied W 5d states of the Keggin unit. Accordingly, the enhanced quantum efficiency can be obtained compared with pure TiO_2 (Scheme 1). The other should be due to the fact that the bandgap of composite films becomes narrow after the introduction of the Keggin unit into the TiO_2 network.

3.8. Mineralization of RB

It is crucial to ensure total mineralization of organic dyes during their photodegradation process since the yielded intermediates may be more toxic than the dye themselves. Therefore, the mineralization of the $H_3PW_{12}O_{40}/TiO_2$ composite film to RB molecule was evaluated by monitoring the changes of TOC in the reaction systems. For comparison, pure TiO_2 film was tested at the same conditions. From Fig. 8 it can be seen that the mineralization of RB over $H_3PW_{12}O_{40}/TiO_2$-14.7 composite films is faster than that of pure TiO_2 film. In the presence of $H_3PW_{12}O_{40}/TiO_2$-14.7, TOC is removed by 77.7% after simulated sunlight irradiation for 12 h. Under the same condition, the mineralization of RB over the pure TiO_2 film takes place at a slower rate; TOC is reduced by 63.3% after simulated sunlight irradiation for 12 h.

3.9. Recyclability of the film catalyst

$H_3PW_{12}O_{40}/TiO_2$-14.7 was chosen to evaluate the regeneration and reusability of the composite film, which is extremely important for the composite film photocatalyst from viewpoint of practical applications. After the first catalytic run, the catalyst was removed and dipped in ethanol for 2 h, and then it was washed with distilled

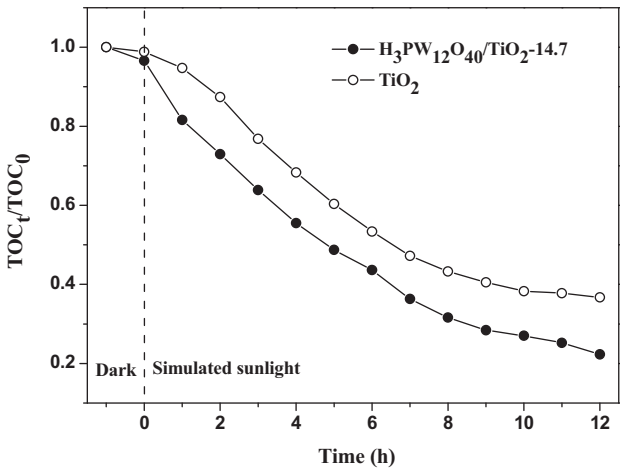

Fig. 8. Evolution of TOC during the course of simulated sunlight photocatalytic degradation of RB over $H_3PW_{12}O_{40}/TiO_2$-14.7 composite film. Initial concentration of RB: 25 mg L^{-1}, volume: 120 mL, catalyst amount: two pieces of quartz (4.5 mg).

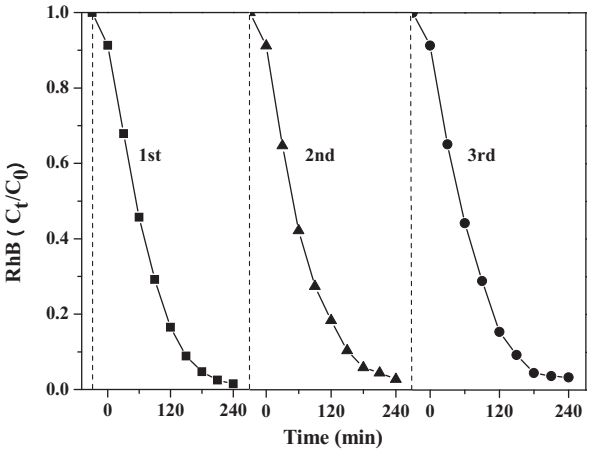

Fig. 9. Recycling runs in the photocatalytic degradation of RB in the presence of $H_3PW_{12}O_{40}/TiO_2$-14.7 composite film. Initial concentration of RB: 25 mg L^{-1}, volume: 120 mL, catalyst amount: two pieces of quartz (4.5 mg).

water and dried at room temperature. The recovered film was used for subsequent two catalytic cycles by using the same regeneration method. From the result depicted in Fig. 9 it is found that the $H_3PW_{12}O_{40}/TiO_2$-14.7 exhibits significantly high catalytic stability, and the activity loss is negligible after three RB degradation cycles (conversion of RB is 98.5%, 97.2%, and 96.7% for the 1st, 2nd, and 3rd catalytic cycle, respectively). Moreover, the used composite film is still in a good condition, and $H_3PW_{12}O_{40}$ loading is 14.0% after three times' catalytic cycles through ICP-AES analysis.

4. Conclusions

The $H_3PW_{12}O_{40}/TiO_2$ composite film photocatalysts with controllable $H_3PW_{12}O_{40}$ loadings were successfully prepared by a sol–gel-hydrothermal treatment-spin-coating route. The composite film exhibited significantly high simulating sunlight photocatalytic activity to dye RB degradation, and its photoactivity outperformed pure TiO_2 film as well as the $H_3PW_{12}O_{40}/TiO_2$ and Degussa P25 TiO_2 powder. This excellent photocatalytic activity of the $H_3PW_{12}O_{40}/TiO_2$ composite film was mainly due to the synergistic effect existed between $H_3PW_{12}O_{40}$ and TiO_2; meanwhile, narrowed bandgap of the composite film with respect to pure TiO_2 also contributed to this unique photocatalytic activity. More importantly, the composite films showed extremely high catalytic stability and maintained the same activity level after three catalytic cycles; additionally, no separation step was needed for the film catalysts and it could be reused after a simple regeneration step. Thereby, as-prepared POM-containing TiO_2 composite film is expected to be a promising photocatalytic material for the practical applications.

Acknowledgements

The authors acknowledge the financial supports from the National Natural Science Foundation of China (50878041; 20873018), the Key Project of Chinese Ministry of Education (308008), the Fundamental Research Funds for the Central Universities (09QNTD004), the Jilin Environmental Protection Bureau (2008–25), the Postdoctoral Science Foundation of China (20090450114; 201003530), and the National Higher-education Institution General Research and Development Project (09SSXT133).

Appendix A. Supplementary data

Supplementary data associated with this article can be found, in the online version, at doi:10.1016/j.jhazmat.2011.08.070.

References

[1] A.L. Linsebigler, G. Lu, J.T. Yates, Photocatalysis on TiO_2 surfaces: principles, mechanisms, and selected results, Chem. Rev. 95 (1995) 735–758.
[2] M.R. Hoffmann, S.T. Martin, W.Y. Choi, D.W. Bahnemann, Environmental applications of semiconductor photocatalysis, Chem. Rev. 95 (1995) 69–96.
[3] A. Fujishima, T.N. Rao, D.A. Tryk, Titanium dioxide photocatalysis, J. Photochem. Photobiol. C: Photochem. Rev. 1 (2000) 1–21.
[4] D. Chatterjee, S. Dasgupta, Visible light induced photocatalytic degradation of organic pollutants, J. Photochem. Photobiol. C: Photochem. Rev. 6 (2005) 186–205.
[5] X. Chen, S.S. Mao, Titanium dioxide nanomaterials: synthesis, properties, modifications, and applications, Chem. Rev. 107 (2007) 2891–2959.
[6] U.I. Gaya, A.H. Abdullah, Heterogeneous photocatalytic degradation of organic contaminants over titanium dioxide: a review of fundamentals, progress and problems, J. Photochem. Photobiol. C: Photochem. Rev. 9 (2008) 1–12.
[7] W. Choi, A. Termin, M.R. Hoffmann, The role of metal ion dopants in quantum-sized TiO_2: correlation between photoreactivity and charge carrier recombination dynamics, J. Phys. Chem. 98 (1994) 13669–13679.
[8] A. Di Paola, E. García-López, S. Ikeda, G. Marcì, B. Ohtani, L. Palmisano, Photocatalytic degradation of organic compounds in aqueous systems by transition metal doped polycrystalline TiO_2, Catal. Today 75 (2002) 87–93.
[9] H. Kisch, S. Sakthivel, M. Janczarek, D. Mitoraj, A low-band gap, nitrogen-modified titania visible-light photocatalyst, J. Phys. Chem. C 111 (2007) 11445–11449.
[10] M. Janus, J. Choina, A.W. Morawski, Azo dyes decomposition on new nitrogen-modified anatase TiO_2 with high adsorptivity, J. Hazard. Mater. 166 (2009) 1–5.
[11] Z. Wu, F. Dong, W. Zhao, S. Guo, Visible light induced electron transfer process over nitrogen doped TiO_2 nanocrystals prepared by oxidation of titanium nitride, J. Hazard. Mater. 157 (2008) 57–63.
[12] O. Akhavan, Thickness dependent activity of nanostructured TiO_2/α-Fe_2O_3 photocatalyst thin films, Appl. Surf. Sci. 257 (2010) 1724–1728.
[13] J. Fang, X.Z. Bi, D.J. Si, Z.Q. Jiang, W.X. Huang, Spectroscopic studies of interfacial structures of CeO_2–TiO_2 mixed oxides, Appl. Surf. Sci. 253 (2007) 8952–8961.
[14] D. Hufschmidt, D. Bahnemann, J.J. Testa, M.I. Litter, Enhancement of the photocatalytic activity of various TiO_2 materials by platinisation, J. Photochem. Photobiol. A: Chem. 148 (2002) 223–231.
[15] C. Hu, Y. Lan, J. Qu, X. Hu, A. Wang, Ag/AgBr/TiO_2 visible light photocatalyst for destruction of azodyes and bacteria, J. Phys. Chem. B 110 (2006) 4066–4072.
[16] A. Hiskia, E. Papaconstantinou, M.C. Bernard, P. Falaras, Influence of metallic silver and of platinum–silver bimetallic deposits on the photocatalytic activity of titania (anatase and rutile) in organic and aqueous media, J. Photochem. Photobiol. A: Chem. 113 (1998) 181–188.
[17] L. Li, Q. Wu, Y. Guo, C. Hu, Nanosize and bimodal porous polyoxotungstate–anatase TiO_2 composites: preparation and photocatalytic degradation of organophosphorus pesticide using visible-light excitation, Micropor. Mesopor. Mater. 87 (2005) 1–9.
[18] D. Carriazo, M. Addamo, G. Marcì, C. Martín, L. Palmisano, V. Rives, Tungstophosphoric acid supported on polycrystalline TiO_2 for the photodegradation of 4-nitrophenol in aqueous solution and propan-2-ol in vapour phase, Appl. Catal. A: Gen. 356 (2009) 172–179.
[19] G. Marcì, E. García-López, L. Palmisano, Photo-assisted degradation of 2-propanol in gas–solid regime by using TiO_2 impregnated with heteropolyacid $H_3PW_{12}O_{40}$, Catal. Today 144 (2009) 42–47.
[20] G. Marcì, E. García-López, L. Palmisano, D. Carriazo, C. Martín, V. Rives, Preparation, characterization and photocatalytic activity of TiO_2 impregnated with the heteropolyacid $H_3PW_{12}O_{40}$: photo-assisted degradation of 2-propanol in gas–solid regime, Appl. Catal. B: Environ. 90 (2009) 497–506.
[21] K. Li, Y. Guo, F. Ma, H. Li, L. Chen, Y. Guo, Design of ordered mesoporous $H_3PW_{12}O_{40}$–titania materials and their photocatalytic activity to dye methyl orange degradation, Catal. Commun. 11 (2010) 839–843.
[22] K. Li, X. Yang, Y. Guo, F. Ma, H. Li, L. Chen, Y. Guo, Design of mesostructured $H_3PW_{12}O_{40}$–titania materials with controllable structural orderings and pore geometries and their simulated sunlight photocatalytic activity towards diethyl phthalate degradation, Appl. Catal. B: Environ. 99 (2010) 364–375.
[23] L. Xu, X. Yang, Y.H. Guo, F.Y. Ma, Y.N. Guo, X. Yuan, M.X. Huo, Simulated sunlight photodegradation of aqueous phthalate esters catalyzed by the polyoxotungstate/titania nanocomposite, J. Hazard. Mater. 178 (2010) 1070–1077.
[24] I.V. Kozhevnikov, Catalysis by heteropoly acids and multicomponent polyoxometalates in liquid-phase reactions, Chem. Rev. 98 (1998) 171–198.
[25] N. Mizuno, M. Misono, Heterogeneous catalysis, Chem. Rev. 98 (1998) 199–217.
[26] Y. Guo, C. Hu, Heterogeneous photocatalysis by solid polyoxometalates, J. Mol. Catal. A: Chem. 262 (2007) 136–148.
[27] S. Fukahori, H. Ichiura, T. Kitaoka, H. Tanaka, Photocatalytic decomposition of bisphenol A in water using composite TiO_2–zeolite sheets prepared by a papermaking technique, Environ. Sci. Technol. 37 (2003) 1048–1051.
[28] A. Conde-Gallardo, M. Guerrero, N. Castillo, A.B. Soto, R. Fragoso, J.G. Cabañas-Moreno, TiO_2 anatase thin films deposited by spray pyrolysis of an aerosol of titanium diisopropoxide, Thin Solid Films 473 (2005) 68–73.

[29] G. Hyett, M. Green, I.P. Parkin, X-ray diffraction area mapping of preferred orientation and phase change in TiO_2 thin films deposited by chemical vapor deposition, J. Am. Chem. Soc. 128 (2006) 12147–12155.
[30] T. Noguchi, A. Fujishima, Photocatalytic degradation of gaseous formaldehyde using TiO_2 film, Environ. Sci. Technol. 32 (1998) 3831–3833.
[31] M. Kitano, M. Takeuchi, M. Matsuoka, J.M. Thomas, M. Anpo, Photocatalytic water splitting using Pt-loaded visible light-responsive TiO_2 thin film photocatalysts, Catal. Today 120 (2007) 133–138.
[32] L. Lei, H.P. Chu, X. Hu, P.L. Yue, Preparation of heterogeneous photocatalyst (TiO_2/alumina) by metallo-organic chemical vapor deposition, Ind. Eng. Chem. Res. 38 (1999) 3381–3385.
[33] C.R. Peterson, E.B. Slamorich, Hydrothermal processing of $PbTiO_3$ and $PbTiO_3$/polymer thin films from titanium metallo-organic precursors, J. Am. Ceram. Soc. 82 (1999) 241–244.
[34] Y. Yang, Y. Guo, C. Hou, E. Wang, Lacunary Keggin-type polyoxometalates-based macroporous composite films: preparation and photocatalytic activity, Appl. Catal. A: Gen. 252 (2003) 305–314.
[35] D. Li, Y. Guo, C. Hu, C. Jiang, E. Wang, Preparation, characterization and photocatalytic property of the $PW_{11}O_{39}^{7-}$/TiO_2 composite film towards azo-dye degradation, J. Mol. Catal. A: Chem. 207 (2004) 183–193.
[36] W. Dong, C.W. Lee, X. Lu, Y. Sun, W. Hua, G. Zhuang, S. Zhang, J. Chen, H. Hou, D. Zhao, Synchronous role of coupled adsorption and photocatalytic oxidation on ordered mesoporous anatase TiO_2–SiO_2 nanocomposites generating excellent degradation activity of RhB dye, Appl. Catal. B: Environ. 95 (2010) 197–207.
[37] C. Roccciccioli-Deltcheff, M. Frank, R. Thouvenot, Vibrational investigations of polyoxometalates. 2. Evidence for anion–anion interactions in molybdenum (VI) and tungsten (VI) compounds related to the Keggin structure, Inorg. Chem. 22 (1983) 207–216.
[38] M.T. Pope, A. Müller, Polyoxometalate chemistry an old field with new dimensions in several disciplines, Angew. Chem. Int. Ed. Engl. 30 (1991) 34–48.
[39] R. Jain, M. Shrivastava, Photocatalytic removal of hazardous dye cyanosine from industrial waste using titanium dioxide, J. Hazard. Mater. 152 (2008) 216–220.
[40] Q. Wang, M. Zhang, C. Chen, W. Ma, J. Zhao, Photocatalytic aerobic oxidation of alcohols on TiO_2: the acceleration effect of a brøsted acid, Angew. Chem. Int. Ed. 49 (2010) 7976–7979.